

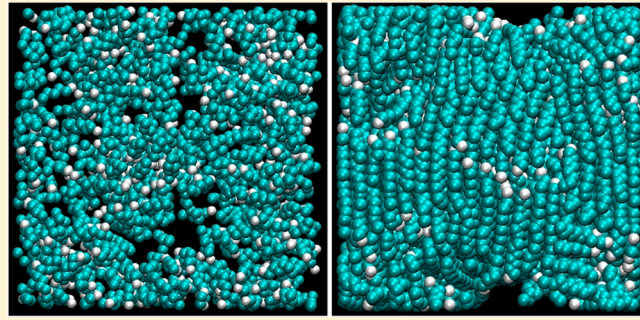
Effect of the Chain Length on the Structure of Ionic Liquids: from Spatial Heterogeneity to Ionic Liquid Crystals

Yumeng Ji,[†] Rui Shi,[†] Yanting Wang,^{†,*} and Giacomo Saielli[‡]

[†]State Key Laboratory of Theoretical Physics, Institute of Theoretical Physics, Chinese Academy of Sciences, 55 East Zhongguancun Road, P.O. Box 2735, Beijing, 100190 China

[‡]Istituto per la Tecnologia delle Membrane del CNR, Unità di Padova, Via Marzolo, 1-35131, Padova, Italy

ABSTRACT: Ionic liquids with intermediate nonpolar cationic side-chain lengths are known to have nanoscale spatial heterogeneities with nonpolar tail domains separated by a continuous polar network. In this work, we use coarse-grained molecular dynamics simulations to show that, when the nonpolar cationic side chain is sufficiently long, due to the stronger van der Waals interactions between the side chains, the structure of ionic liquids goes through a transition from spatially heterogeneous to liquid crystalline-like. For XMIm⁺/NO₃⁻ ionic liquids, change occurs when the number of carbon groups on the cationic side chain varies from 14 to 16. In the liquid crystal-like phase, the cationic side chains tend to be parallel to each other, while the cationic head groups and anions, although being mostly layered perpendicularly to the direction along the side chains, still form a continuous polar network.



1. INTRODUCTION

Because of their unique features, that is being both ionic and organic, ionic liquids have perspective wide applications in many areas, including solar cell,^{1,2} optoelectronic device,³ and organized reaction media.⁴ Several years ago, molecular dynamics (MD) simulations^{5–7} discovered the spatially heterogeneous structure in room-temperature ionic liquids (ILs) whose nonpolar cationic side chains usually contain less than 14 carbon groups. In this microscopic picture, the charged cationic head groups and the anions form a continuous polar network, while the alkyl side chains are pushed by the polar network to aggregate and form separated nonpolar tail domains. Many experimental results (see, e.g., refs 8–12) suggest that ILs with intermediate nonpolar side-chain lengths may really have this nanoscale spatial heterogeneity. At the same time, many other experiments^{4,13,14} indicated that liquid crystal (LC) phases exist for ILs with long side chains. As expected for long chain amphiphilic molecules, because of microsegregation effects the LC phases formed are layered, thus of smectic (Sm) type.^{15,16} Several different smectic phases have been observed in ILCs: SmA,¹⁷ SmB,¹⁸ SmC,¹⁹ SmE,²⁰ and SmT.²⁰ In particular, 1-alkyl-3-methylimidazolium nitrates have been found to have a bilayered smectic A phase.^{4,21} The remaining question is, around room temperature, what the mechanism is for ILs to change from spatially heterogeneous liquid to liquid crystalline structures when the alkyl side-chain length increases.

Because of many experimental difficulties, currently computer simulations might be the only possible way to explore the answer for the above question. However, the all-atom molecular

simulations with current computer power are still not capable of investigating those difficult problems because of the large spatial scale required by the lengthiness of the ionic liquid crystal (ILC) molecules and the long temporal scale required by the high viscosity of ILCs. For example, in ref 22, [C₈Mim][C₈SO₃] was investigated by atomistic MD simulations and only the incipient formation of layers resembling the experimentally observed smectic A phase was observed. Recently, Voth et al. developed the effective force coarse-graining (EF-CG) methodology²³ and applied it to developing a transferable CG model for the XMIm⁺/NO₃⁻ ILs.²⁴ The advantage of MD simulations utilizing the EF-CG model is not only the greatly reduced spatial degrees of freedom, but also the accelerated dynamics. By employing this EF-CG model, one of us performed CG MD simulations for the ILC 1-methyl-3-hexadecylimidazolium nitrate, C₁₆MIm⁺/NO₃⁻.²⁵ However, it still remains an unsolved and very important issue how the lengthening of the alkyl chain drives the appearance and stabilization of an ionic smectic phase.

In this work, we perform the CG MD simulations for the XMIm⁺/NO₃⁻ ILs with various side-chain lengths ranging from 6 to 22 carbon groups by employing the transferable EF-CG model²⁴ to study how the ILs change from the spatially heterogeneous structure to liquid crystalline-like with increasing cationic side-chain length. It should be mentioned that transferability of coarse-grained potential into different phases

Received: October 16, 2012

Revised: January 6, 2013

Published: January 10, 2013

is not granted even if the selected model is transferable with temperature.²⁶ However, the previous MD investigation²⁵ ensures that the EF-CG model potential exhibits a smectic phase. Our simulation results suggest that, in the ILC-like phase, the cationic side chains tend to parallel to each other, while the charged cationic head groups and the anions, like in the spatially heterogeneous phase, still form a continuous polar network, despite the fact that the charge density distribution is layered. A sharp decrease of the spatial heterogeneity of the tail groups is found when the number of side-chain carbon groups changes from 14 to 16, in qualitative agreement with experimental observations,^{4,13,14,21,27} indicating that, when the side chain is adequately long, the cationic nonpolar tails do not aggregate to form separated tail domains, but instead line up to generate liquid crystalline-like layers.

2. SIMULATION METHODS

By utilizing the transferable EF-CG model which can satisfactorily rebuild the structural properties,²⁴ CG MD simulations were performed for $C_n\text{MIm}^+/\text{NO}_3^-$ with $n = 6, 8, \dots, 22$ to obtain their equilibrium structures at the temperature $T = 400$ K. As shown in Figure 1, the EF-CG strategy groups

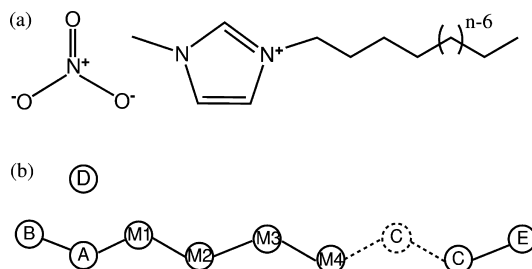


Figure 1. (a) Atomistic molecular structure and (b) coarse-grained model of $\text{C}_n\text{MIm}^+/\text{NO}_3^-$.

the imidazolium ring into a single CG site A, the anion site D, the single methyl group site B, the terminal methyl group site E, the charged methylene groups connected to the imidazolium ring sites M1, M2, M3, and M4, ordered from the cationic ring to the terminal of the side chain, and all charge-neutral methylene groups on the side chain sites C. The studied IL systems only differ from the number of sites C on their cationic side chains, and share the same transferable EF-CG force field at the CG level. Details of the EF-CG model can be found in ref 24.

The initial configurations for the IL systems were generated as follows. For each type of IL, the all-atom configuration of a single cation was drawn with GaussView,²⁸ which was converted to the CG representation. The CG configuration of the cation, along with site D (anion), was then duplicated 512 times and uniformly located on the lattice positions in an adequately large simulation box. The constructed initial configurations then went through a simulated annealing²⁹ procedure with the DL_POLY 2 MD simulation package³⁰ by the following steps: (1) with the pressure $P = 20$ atm and $T = 400$ K, the initial configurations went through a constant NPT MD simulation for 10^6 steps to suppress the system volume; (2) a constant NPT MD simulation for 10^6 steps with $P = 1$ atm and $T = 400$ K was followed for equilibration and another subsequent 10^6 steps were simulated to sample the average size of the simulation box; (3) with the simulation size fixed at the value determined by the previous step, the system temperature

was increased to $T = 2000$ K to perform a constant NVT MD simulation for 200 ps, and then sequentially decreased to 1500, 1000, 700, 500, and 400 K with the simulation durations of 300 ps, 500 ps, 1 ns, 2 ns, and 20 ns, respectively; (4) a 10-ns constant NVT MD simulation at $T = 400$ K was followed to collect data with a sampling interval of 1000 steps. In all the above MD simulations, the time step was set to be 4 fs. The simulated annealing procedure allows the system to relax adequately and converge with a very large probability to the global minimum structure, subject to the limitation of simulation time, system size, and simulation box shape. In all the simulations, the temperature and pressure were kept constant using the Nosé–Hoover thermostat³¹ and the Hoover barostat,³² respectively. The cutoff distances for the electrostatic and van der Waals (VDW) interactions were set to be 14 Å and the Ewald summation was used to treat the electrostatic interactions. It should be noted that the cubic simulation box shape might not be suitable for simulating a liquid crystal phase, which is structurally anisotropic. Here we still employ a cubic one because we want to make a direct comparison with the previously simulated spatial heterogeneity phase, which has been done with a cubic simulation box.^{5,6,33} As shown by our simulation results reported below, the ILC domains still form with the cubic simulation box regardless of the distortion induced by the box shape. In this way, we may see more clearly the structural transition and what is the mechanism driving the growth of the smectic layers from the spatially heterogeneous phase as the chain length increases, rather than the detailed structure of ILC itself.

3. RESULTS AND DISCUSSION

From now on, we use C_n to denote the $\text{C}_n\text{MIm}^+/\text{NO}_3^-$ IL system, and *head* refers to CG site A, *anion* refers to CG site D, *tail* refers to CG site E, *polar groups* refers to CG sites A and D, and *nonpolar groups* refers to the uncharged carbon groups on side chains. Two randomly chosen snapshots of equilibrated C_{10} and C_{22} , respectively, are shown in Figure 2. It can be clearly seen that C_{10} forms nonpolar tail domains separated by the continuous polar network, while C_{22} has the side chains lined up along the Z direction to form a smectic phase, but the bundles of side chains slightly tilt in different ways. Although the polar groups are more layered in C_{22} than in C_{10} due to the lineup of the side chains, as seen in Figure 2, because of strong attractive electrostatic interactions, they still form a continuous polar network. The difference is that, for C_{22} , most polar groups are inside layered planes, so only a few polar groups are in between to bridge the polar groups in layer.

The heterogeneity order parameter (HOP)³³ was calculated for different IL systems to quantify the structural change from the spatially heterogeneous structure to the liquid crystalline structure. The HOP is defined as

$$\hat{h} = \frac{1}{N_s} \sum_{i=1}^{N_s} \sum_{j=1}^{N_s} \exp(-r_{ij}^2/2\sigma^2) \quad (1)$$

where r_{ij} is the modulus of the vector connecting sites i and j , corrected for periodic boundary conditions, and $\sigma = L/N_s^{1/3}$ with L the side length of the cubic simulation box and N_s the total number of sites. Because a shorter distance between two sites has a larger weight, the HOP value is larger when more sites are closer in space.

From Figure 3a we can see that the HOP of tail groups increases from C_6 to C_{14} . Because the increased number of

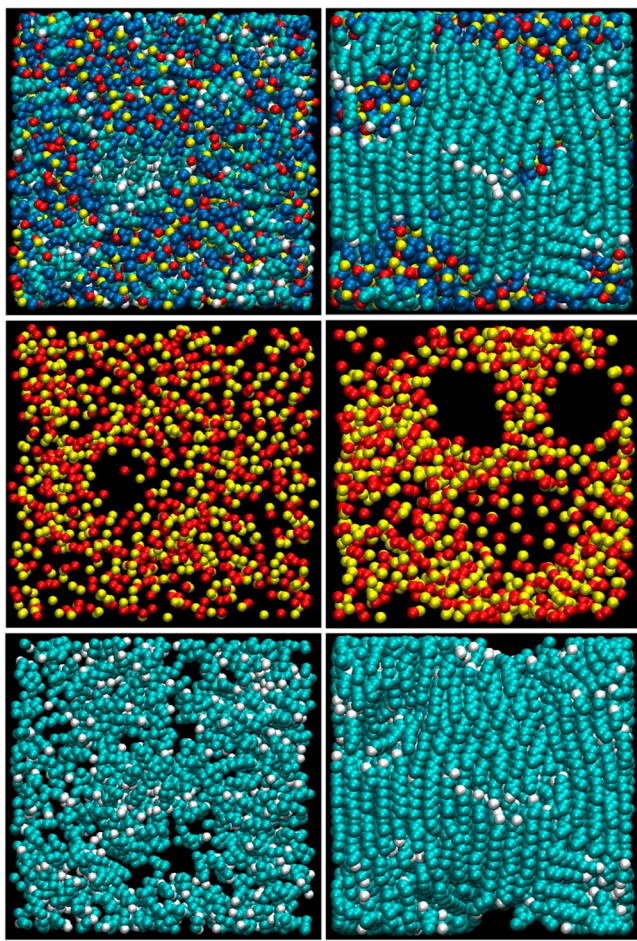


Figure 2. Random snapshots of C_{10} (left column) and C_{22} (right column). Key: first row, all CG sites; second row, polar groups (CG sites A and D) only; third row, nonpolar groups (CG sites C and E) only. The coloring scheme is as follows: CG sites A, yellow; CG sites B, M1, M2, M3, and M4, blue; CG sites C, cyan; CG sites D, red; CG sites E, white.

carbon groups requires more space, the alkyl side chains aggregate more tightly with increasing side-chain length. Correspondingly, the polar groups are pushed by the nonpolar groups to pack more closely, resulting in the increase of their HOP values. On the other hand, for C_{16} to C_{22} , the VDW interactions between side chains are so strong that the lineup of nonpolar side chains becomes energetically preferable over tail aggregation, leading to an ILC-like structure. Because in the ILC-like structure, the terminal groups of the side chains distribute roughly uniformly in various layers, the HOP of tail

groups decreases drastically from C_{14} to C_{16} . In the ILC region, the side chains elongate along the Z axis and has less effect on the compactness of the polar groups, thus their HOP values only increase very slowly. The HOP values for the tail groups clearly show that the IL systems of C_6 to C_{14} belong to the spatially heterogeneous region, while those of C_{16} to C_{22} belong to the ILC region.

This change in the structural arrangement of the alkyl chains occurring at C_{14} is in remarkable agreement with the experimental observation that smectic phases in alkylimidazolium nitrates can only be formed for alkyl chain lengths at least of C_{14} .²¹ Therefore, the interaction between the alkyl chains play a fundamental role in determining the type of ionic phase formed.

To verify that the nonpolar side chains are indeed parallel to their neighbors, we defined and calculated the *orientation correlation function* (OCF) for side chains. For each cation, the orientation of the side chain is represented by the orientation of the vector pointing from site A to site E. The OCF is defined as the ensemble-averaged correlation between the orientations of two side chains as a function of the distance between the center of mass of cations:

$$C(r) = \langle [3(\hat{u}(\vec{r}_i) \cdot \hat{u}(\vec{r}_j))^2 - 1] \cdot \delta(\vec{r} - \vec{r}_i + \vec{r}_j)/2 \rangle \quad (2)$$

where $\hat{u}(\vec{r}_i)$ is the unit vector pointing from site A to site E of cation i that located at position \vec{r}_i . As seen from Figure 3b, the OCFs for various IL systems all reach their maximal values at around 4.8 Å, which is roughly the distance between two cationic side chains. Therefore, the maximal value of the OCF represents the orientation correlation between the side chains of the two nearest cations. In the range of the spatially heterogeneous structure from C_6 to C_{14} , the maximal value of the OCF increases with the side-chain length because of the increased degree of aggregation. Once the structure is transformed to ILC-like (C_{16} to C_{22}), the correlation between the nearest cations is close to 1 and does not change much, since the side chains are now parallel to each other. With increasing distance, the OCF values for C_6 to C_{14} gradually decrease to zero, because in the tail-aggregation structure, the side chains do not have long-range correlations. In contrast, the OCF values for C_{16} to C_{22} gradually decrease to a finite value, indicating that the ILC-like structure does have a long-range order for side chains. On the other hand, the decrease of the correlation with distance indicates that the side chains are not perfectly parallel to each other as in an ideal smectic liquid crystal structure, which can be partly ascribed to the presence of different smectic-like domains in the simulation box.

The radial distribution functions (RDFs) were calculated to further quantify the structural properties of ILs. As shown in

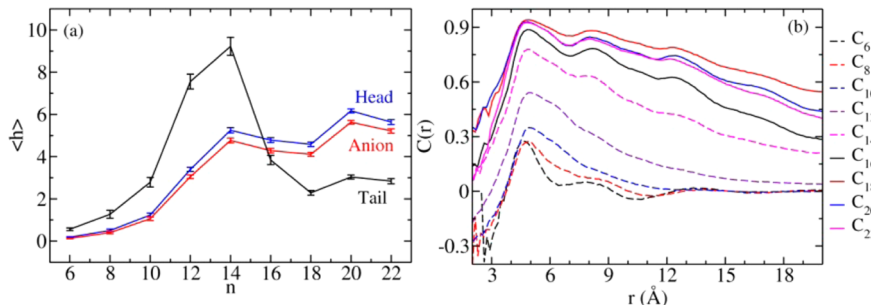


Figure 3. (a) Heterogeneity order parameters for CG sites A (head), D (anion), and E (tail). (b) Orientation correlation functions for side chains.

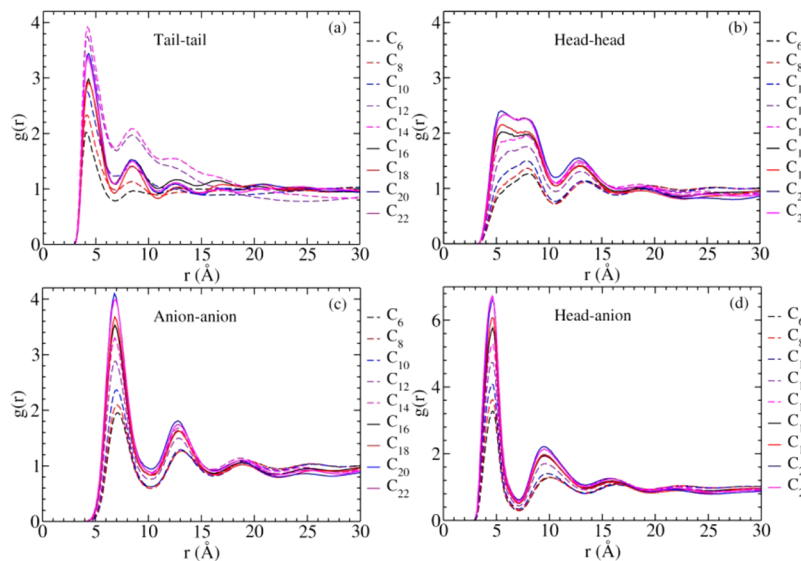


Figure 4. Radial distribution functions of tail–tail (a), head–head (b), anion–anion (c), and head–anion (d).

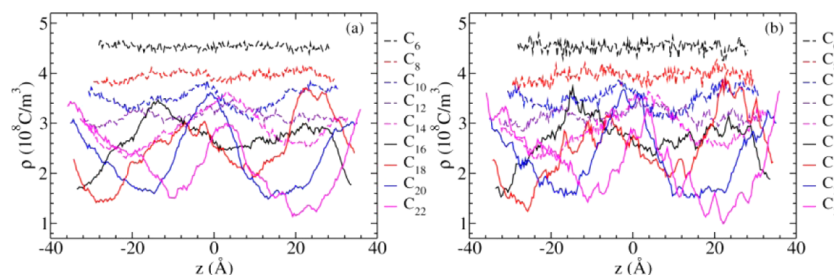


Figure 5. Charge layering of (a) positive and (b) negative charges along the Z direction, in which the side chains line up.

Figure 4a, consistent with the HOP values for the tail groups, the first peak of the tail–tail RDF increases quickly from C_6 to C_{14} , then drops down significantly at C_{16} , and increases again slowly from C_{16} to C_{22} . Because the side chains are layered in the ILC region, the tail–tail RDFs for C_{16} to C_{22} have more peaks than those for C_6 to C_{14} . Also consistent with the HOP values, the first peaks of the RDFs between polar groups increase roughly monotonically from C_6 to C_{22} , attributed to the increased volume exclusion of the side chains. For C_{16} – C_{22} , a peak appears at 5 Å in the head–head RDFs and grows as the length of side chain increases because in the ILC phase, the side chains are bundled together and the head groups tend to stay close with each other in the same layer. It should be noted that the details of our head–head RDFs might differ from all-atom ones since in our CG scheme, the whole planar head ring has been coarse-grained as a single CG site. Nevertheless, we believe the qualitative conclusions based on the CG head–head RDFs are still valid.

To see the layering of the polar groups more clearly, we calculated the positive and negative charge densities along the Z direction, which turns out to be the direction where most of the smectic domains align; the results are plotted in Figure 5. The charge distributions are uniform along the X and Y directions for all systems (data not shown). Along the Z direction, the charges are almost uniformly distributed for C_6 , slightly layered for C_8 to C_{14} , and significantly layered into two layers for C_{16} to C_{22} . Because the positively and negatively charged atomic groups mostly stay close to each other due to strong

electrostatic interactions, their charge distributions are almost identical for all the IL systems.

To verify that the structural transition is indeed invoked by the increment of the VDW attractions, the VDW and electrostatic potential energy values for all IL systems have been calculated and are listed in Table 1. With increasing alkyl

Table 1. Electrostatic and VDW Potential Energies as a Function of Alkyl Chain Length^a

chain length	E_{VDW}	ΔE_{VDW}	E_{elec}
6	-135.0 ± 4.1	0.0	-2335.6 ± 3.5
8	-199.8 ± 4.4	-64.8	-2330.3 ± 3.9
10	-261.7 ± 4.5	-61.9	-2333.2 ± 3.8
12	-323.6 ± 4.6	-61.9	-2347.1 ± 3.8
14	-404.8 ± 5.6	-81.2	-2350.7 ± 3.9
16	-503.1 ± 4.9	-98.3	-2340.1 ± 3.6
18	-603.0 ± 4.7	-99.9	-2335.1 ± 3.9
20	-676.0 ± 4.7	-73.0	-2342.6 ± 3.7
22	-756.2 ± 4.8	-80.2	-2337.4 ± 3.8

^aEnergies are in eV.

side-chain length, the attractive VDW potential energy increases very quickly due to the increased number of nonpolar carbon groups on side chains, while the electrostatic energy does not vary much. Moreover, comparing the VDW energy differences (ΔE_{VDW}) between adjacent chain length systems, we found that ΔE_{VDW} remains around -63 eV for C_8 , C_{10} , and C_{12} , and decreases to -81.2 eV for C_{14} , and then further

decreases to about -99 eV for C_{16} and C_{18} . ΔE_{VDW} slightly increases for C_{20} and C_{22} , possibly due to the deviation from a perfect smectic A phase as a result of employing the cubic simulation box. Since the alignment of side chains favors a decrease of ΔE_{VDW} , this trend again implies a structural transition when the chain length increases: in the spatially heterogeneous phase, ΔE_{VDW} keeps a high value because the side chains aggregate disorderly, and it gradually decreases in the ILC phase due to the alignment of side chains. Thus, the jump in ΔE_{VDW} cannot be attributed simply to the increased chain length, rather to a different structural arrangement and it is noteworthy that it occurs around C_{14} , consistent with the change of OCF (See Figure 3b), therefore confirming that this mechanism is a key feature driving the formation of the ionic mesophase. Therefore, we believe the increasing attractive VDW interactions drive the alkyl side chains to be parallel to each other and thus induce the structural transition from spatially heterogeneous to ILC-like.

4. CONCLUSIONS

In conclusion, by increasing the alkyl cationic side-chain length in our CG MD simulations, we observed a transition from the known spatially heterogeneous structure to an ILC-like structure due to the increased VDW interactions between cationic side chains. Coincident with the experimental observations,⁴ the ILC-like structure obtained by our simulation is close to smectic A, since the layers formed by the side chains are roughly perpendicular to the direction in which the side chains are parallel to each other, which is also supported by the layering of the charges along the same direction. Although layered, due to strong electrostatic interactions, the polar groups still form a continuous polar network.

From the energetic point of view, the transition from the spatially heterogeneous structure to the ILC-like structure results from the competition between the electrostatic interactions between polar groups and the VDW interactions between side chains. For the C_2 system, since the electrostatic interactions dominate and the VDW interactions between side chains are relatively small, only very weak instantaneous spatial heterogeneity was observed in MD simulation.^{34,35} For C_6 to C_{14} , the collective VDW interactions between side chains are stronger, but still weaker than the electrostatic interactions between polar groups. Consequently, the polar groups form a continuous polar network and push the nonpolar side chains to aggregate and form separated tail domains.³⁶ For C_{16} to C_{22} , the VDW interactions between side chains are competitive to the electrostatic interactions between polar groups, so the side chains have to arrange in order by paralleling to each other to lower the total free energy. Nevertheless, although forced to be layered by the ordering of the side chains, the polar groups still have relatively strong electrostatic interactions to form a continuous polar network. We expect that, when the cationic nonpolar side chains are extraordinarily long, the VDW interactions between side chains dominate and the polar groups can no longer form a global continuous polar network. Consequently, the IL systems are more like charged polymers and form a regular smectic-A phase. MD simulations with a much larger size are required to verify our prediction of the regular smectic-A phase.

The analysis of dynamic properties, which is missing in our current work, would certainly provide more information about the transition from spatially heterogeneous to liquid crystalline-like. However, since the EF-CG method has been designed to

rebuild satisfactory structural properties rather than dynamic properties, it is difficult to analyze the dynamic properties based on our current CG MD simulations, and the investigation of the dynamics properties for ILC will be the subject of our future work.

■ AUTHOR INFORMATION

Corresponding Author

*E-mail: wangyt@itp.ac.cn.

Notes

The authors declare no competing financial interest.

■ ACKNOWLEDGMENTS

This work was supported by the National Natural Science Foundation of China (No. 10974208 and No. 11121403) and the Hundred Talent Program of the Chinese Academy of Sciences (CAS). The authors thank the Supercomputing Center in the Computer Network Information Center at the CAS for allocations of computer time. G.S. thanks the CAS-CNR bilateral agreement (2011–2013) for sponsoring a visit to ITP-CAS, and MIUR (PRIN 20085M27SS, FIRB RBAP11C58Y) and Fondazione CARIPARO (NanoMode 2010) for support.

■ REFERENCES

- (1) Yamanaka, N.; Kawano, R.; Kubo, W.; Kitamura, T.; Wada, Y.; Watanabe, M.; Yanagida, S. *Chem. Commun.* **2005**, 740–742.
- (2) Yamanaka, N.; Kawano, R.; Kubo, W.; Masaki, N.; Kitamura, T.; Wada, Y.; Watanabe, M.; Yanagida, S. *J. Phys. Chem. B* **2007**, 111, 4763–4769.
- (3) Haristoy, D.; Tsiorvas, D. *Chem. Mater.* **2003**, 15, 2079–2083.
- (4) Lee, C. K.; Huang, H. W.; Lin, I. J. B. *Chem. Commun.* **2000**, 1911–1912.
- (5) Wang, Y.; Jiang, W.; Voth, G. A. Spatial Heterogeneity in Ionic Liquids. In *Ionic Liquids IV: Not Just Solvents Anymore*; Brennecke, J. F., Rogers, R. D., Seddon, K. R., Eds.; American Chemical Society: Washington, DC, 2007; Vol. 975; pp 272–307.
- (6) Wang, Y.; Voth, G. A. *J. Am. Chem. Soc.* **2005**, 127, 12192–12193.
- (7) Canongia Lopes, J. N. A.; Pádua, A. A. H. *J. Phys. Chem. B* **2006**, 110, 3330–3335.
- (8) Triolo, A.; Russina, O.; Bleif, H.-J.; Di Cola, E. *J. Phys. Chem. B* **2007**, 111, 4641–4644.
- (9) Xiao, D.; Rajian, J. R.; Cady, A.; Li, S.; Bartsch, R. A.; Quitevis, E. L. *J. Phys. Chem. B* **2007**, 111, 4669–4677.
- (10) Turton, D. A.; Hunger, J.; Stoppa, A.; Hefter, G.; Thoman, A.; Walther, M.; Buchner, R.; Wynne, K. *J. Am. Chem. Soc.* **2009**, 131, 11140–11146.
- (11) Iwata, K.; Okajima, H.; Saha, S.; Hamaguchi, H.-o. *Acc. Chem. Res.* **2007**, 40, 1174–1181.
- (12) Russina, O.; Triolo, A.; Gontrani, L.; Caminiti, R. *J. Phys. Chem. Lett.* **2011**, 3, 27–33.
- (13) Holbrey, J. D.; Seddon, R. K. *J. Chem. Soc., Dalton Trans.* **1999**, 2133–2140.
- (14) Gordon, C. M.; Holbrey, J. D.; Kennedy, A. R.; Seddon, R. K. *J. Mater. Chem.* **1998**, 8, 2627–2636.
- (15) Axenov, K. V.; Laschat, S. *Materials* **2011**, 4, 206–259.
- (16) Causin, V.; Saielli, G. In *Green Solvents II. Properties and Applications of Ionic Liquids*; Mohammad, A., Inamuddin, D., Eds.; Springer: London, 2012; p 79.
- (17) Kouwer, P. H. J.; Swager, T. M. *J. Am. Chem. Soc.* **2007**, 129, 14042–14052.
- (18) Causin, V.; Saielli, G. *J. Mater. Chem.* **2009**, 19, 9153–9162.
- (19) Starkulla, G. F.; Klenk, S.; Butschies, M.; Tussetschlager, S.; Laschat, S. *J. Mater. Chem.* **2012**, 22, 21987–21997.

- (20) Goossens, K.; Lava, K.; Nockemann, P.; Van Hecke, K.; Van Meervelt, L.; Driesen, K.; Görller-Walrand, C.; Binnemans, K.; Cardinaels, T. *Chem.—Eur. J.* **2009**, *15*, 656–674.
- (21) Guillet, E.; Imbert, D.; Scopelliti, R.; Bünzli, J.-C. G. *Chem. Mater.* **2004**, *16*, 4063–4070.
- (22) Blesic, M.; Swadzba-Kwasny, M.; Holbrey, J. D.; Canongia Lopes, J. N.; Seddon, K. R.; Rebelo, L. P. N. *Phys. Chem. Chem. Phys.* **2009**, *11*, 4260–4268.
- (23) Wang, Y.; Noid, W. G.; Liu, P.; Voth, G. A. *Phys. Chem. Chem. Phys.* **2009**, *11*, 2002–2015.
- (24) Wang, Y.; Feng, S.; Voth, G. A. *J. Chem. Theor. Comput.* **2009**, *5*, 1091–1098.
- (25) Saielli, G. *Soft Matter* **2012**, *8*, 10279–10287.
- (26) Mukherjee, B.; Delle Site, L.; Kremer, K.; Peter, C. *J. Phys. Chem. B* **2012**, *116*, 8474–8484.
- (27) Bradley, A. E.; Hardacre, C.; Holbrey, J. D.; Johnston, S.; McMath, S. E. J.; Nieuwenhuyzen, M. *Chem. Mater.* **2002**, *14*, 629–635.
- (28) Frisch, A.; Nielsen, A. B.; Holder, A. J. *Gaussview User Manual*; Gaussian Inc.: Pittsburgh, PA, 2001.
- (29) Kirkpatrick, S.; Gelatt, C. D.; Vecchi, M. P. *Science* **1983**, *220*, 671–680.
- (30) Forester, T. R.; Smith, W. *DL_POLY User Manual*; CCLRC, Daresbury Laboratory: Daresbury, Warrington, U.K., 1995.
- (31) Hoover, W. G. *Phys. Rev. A* **1985**, *31*, 1695–1697.
- (32) Melchionna, S.; Ciccotti, G.; Holian, B. L. *Mol. Phys.* **1993**, *78*, 533–544.
- (33) Wang, Y.; Voth, G. A. *J. Phys. Chem. B* **2006**, *110*, 18601–18608.
- (34) Yan, T.; Wang, Y.; Knox, C. *J. Phys. Chem. B* **2010**, *114*, 6905–6921.
- (35) Yan, T.; Wang, Y.; Knox, C. *J. Phys. Chem. B* **2010**, *114*, 6886–6904.
- (36) Zhao, H. Q.; Shi, R.; Wang, Y. T. *Commun. Theor. Phys.* **2011**, *56*, 499–503.